Minimum Mass Cast Glass Structures Under Performance and Manufacturability Constraints

Koniari, A.M.; Andriotis, C.; Oikonomopoulou, F.

DOI
10.1007/978-3-031-37189-9_29

Publication date
2023

Document Version
Final published version

Published in
Computer-Aided Architectural Design. INTERCONNECTIONS: Co-computing Beyond Boundaries.

Citation (APA)
Koniari, A. M., Andriotis, C., & Oikonomopoulou, F. (2023). Minimum Mass Cast Glass Structures Under Performance and Manufacturability Constraints. In M. Turrin, C. Andriotis, & A. Rafiee (Eds.), *Computer-Aided Architectural Design. INTERCONNECTIONS: Co-computing Beyond Boundaries.* (pp. 437-451). (Communications in Computer and Information Science; Vol. 1819). Springer. https://doi.org/10.1007/978-3-031-37189-9_29

Important note
To cite this publication, please use the final published version (if applicable).
Please check the document version above.

Michela Turrin
Charalampos Andriotis
Azarakhsh Rafiee (Eds.)

Communications in Computer and Information Science 1819

Computer-Aided Architectural Design

INTERCONNECTIONS: Co-computing Beyond Boundaries

20th International Conference, CAAD Futures 2023
Delft, The Netherlands, July 5–7, 2023
Selected Papers

TU Delft
Springer
MOREMEDIA

Michela Turrin · Charalampos Andriotis ·
Azarakhsh Rafiee
Editors

Computer-Aided Architectural Design

INTERCONNECTIONS: Co-computing Beyond Boundaries

20th International Conference, CAAD Futures 2023
Delft, The Netherlands, July 5–7, 2023
Selected Papers

Springer

Editors
Michela Turrin
Delft University of Technology
Delft, The Netherlands

Charalampos Andriotis
Delft University of Technology
Delft, The Netherlands

Azarakhsh Rafiee
Delft University of Technology
Delft, The Netherlands

ISSN 1865-0929 ISSN 1865-0937 (electronic)
Communications in Computer and Information Science
ISBN 978-3-031-37188-2 ISBN 978-3-031-37189-9 (eBook)
https://doi.org/10.1007/978-3-031-37189-9

This Springer imprint is published by the registered company Springer Nature Switzerland AG
The registered company address is: Gewerbestrasse 11, 6330 Cham, Switzerland

Contents

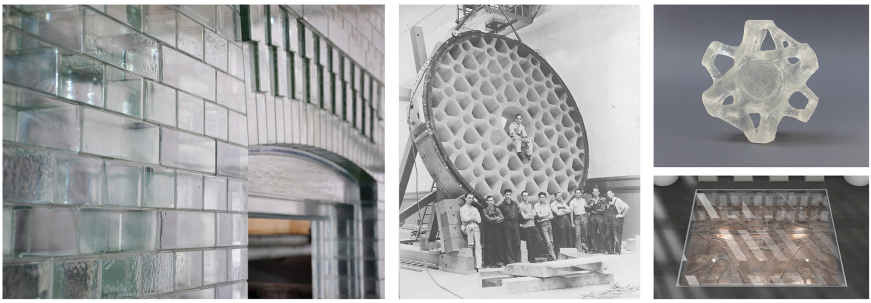

Fig. 1. (from left to right) The Crystal Houses façade made of cast glass bricks/Mirror of Mt. Palomar telescope. Image source: Collection of the Rakow Research Library, The Corning Museum of Glass/Glass node (top) and floor (bottom) designed with TO. Image source: [2].

elements that escape the two-dimensionality of float glass panes and fully exploit the glass properties, such as the great compressive strength, which is higher than that of conventional building materials, including wood, steel, and concrete [1].

Yet, the vast shaping potential of cast glass has, so far, been little explored in structural applications in architecture, hindered mainly by the lengthy annealing[1] process that renders their production unrealistic because of the corresponding high energy and manufacturing costs [1, 2, 3]. The selected structural geometry and glass composition are the most critical factors for the annealing time needed [1]. Essentially, the annealing time increases exponentially when selecting a glass composition with higher thermal expansion coefficient or when enlarging the cross-sectional dimension of a glass component [2, 4]. In the latter case, this results in limiting the existing architectural cast glass applications only to structures made of small glass bricks (Fig. 1, left), so that the cross-sectional dimensions can be cooled down in a reasonable time [5, 6].

However, the optimization of the stiffness-to-weight ratio of cast glass structures and/or the use of glass types with a lower thermal expansion coefficient can greatly reduce the annealing time needed allowing for larger overall dimensions [1]. The benefits of applying these strategies have been well demonstrated by the cast glass honeycomb mirror blanks of the giant telescopes (Fig. 1, middle), since dimensions up to 8.4 m in diameter have been achieved [7, 8] in a considerably reduced annealing time.

In this regard, Topology Optimization (TO) has large potential for the design of massive cast glass structures (Fig. 1, right), since it allows to reach structural forms that maximize stiffness with minimal mass and sparse geometries [2, 3]. This furnishes additional benefits in fabrication time, embodied energy, and cost efficiency making such structures feasible to manufacture. Previous research utilizing commercial TO software successfully demonstrates the ability to engineer glass components of minimum mass, although it highlights the incompatibility of such TO software for the design with glass as structural material [2, 3]. This derives from the fact that such software is developed for conventional, mainly ductile, building materials and, thus, does not fully incorporate

[1] The cooling process consists of phases with different cooling rates [4]. In this paper, only annealing is going to be considered since it is the lengthiest of all cooling phases, thus, having the larger effect on the total time needed.

neither manufacturing constraints linked to annealing nor asymmetric principal stress constraints, that reflect the brittle nature of glass, in the formulation [2, 3]. In this light, this study investigates how the optimization problem can be formulated so that it particularly addresses the annealing time constraint, following similar approaches that have recently been developed in the direction of integrating manufacturing limitations in TO formulations for the creation of realistic algorithmic design workflows [9, 10].

Regarding structural performance, the most critical factor in glass structures is tension since, besides its considerably lower strength value, accounting for less than 10% of the respective compressive strength, it can activate different fracture mechanisms in the component leading to failure even before the tensile stress reaches its allowable limit [6]. Therefore, it is essential that an individual evaluation of both principal stresses is incorporated into the TO formulation to converge into feasible results.

The integration of principal stress constraints within TO formulations is considered either with global stress values [11, 12, 13, 14] or with local evaluation of stresses in each finite element. The latter has been proven to be more effective in the elimination of peak values converging, therefore, to more realistic results [13, 15, 16, 17]. However, there are inherent challenges in the integration of stress constraints into the optimization problem, related mainly to the large computational time needed. Thus, the evaluation of stresses is usually linked to the application of material failure criteria and, particularly, the Von mises criterion [11, 12, 13, 14, 15, 17, 18] which refers to ductile materials. Regarding brittle materials, there are approaches which either investigate the asymmetric stress behavior through the application of the Drucker-Prager criterion [19, 20, 21] or apply unified functions that can serve different failure criteria [16].

This paper addresses the aforementioned challenges of (i) annealing-related manufacturing constraints and (ii) asymmetric principal stress criteria within a uniform mathematical formulation for the establishment of a method that will contribute to the efficient design of monolithic glass structures that are feasible to fabricate taking into full consideration the mechanical properties of glass. To do so, we develop a nonlinear programming formulation within the concept of penalized artificial density interpolation [22] to optimize planar structural profiles. Accordingly, the solution algorithm code is coupled with plane stress quadrilateral finite elements and the optimization problem is solved with the interior-point method.

2 Problem Statement

The optimization problem refers to a planar design domain Ω_{des} modeled with quadrilateral finite elements, formulated within the penalized density interpolation scheme as introduced in [22]. In this regard, the stiffness of each finite element is expressed in function of a pseudo-density value ρ_e which reflects the existence or absence of material, such as:

$$E(\rho_e) = E_0 + \rho_e^p (E - E_0) \tag{1}$$

$$0 < \rho_{min} \leq \rho_e \leq 1, \quad e \in \Omega_{des} = \Omega_{mat} \subseteq R^n, \; n = 2$$

where p is the penalization value; E is the Young's modulus of the material; E_0 and ρ_{min} are lower bounds for stiffness and pseudo-density, respectively, in order to avoid singularities of void elements; and Ω_{mat} is the total material domain. Given that non-design domain is not considered, Ω_{des} equals Ω_{mat}.

Additionally, a filtering technique is applied to address inherent numerical issues in TO such as the checkerboard problem [23, 24], which can result into unrealistic shapes. The adopted formulation applies a technique similar to image processing where the pseudo-density value of each element is derived as a weighted average of the element values inside a fixed neighborhood [23]. Instead of the compliance-based approach [14, 21, 23, 24, 25, 26], in this paper the formulation is volume-based since it reflects better the posed problem of minimizing the mass, and has been proven to result in robust solutions [13, 17, 19, 20]. Thus, the objective is formulated as:

$$\min V = \int_{\Omega_{des}} t\rho_e d\Omega, \quad e \in \Omega_{des} = \Omega_{mat} \subseteq R^n, \; n = 2 \tag{2}$$

where t is the thickness of the structure.

In total, six different types of constraints are applied in the TO formulation. The structural constraints refer to global equilibrium, compliance, displacement, and principal stresses (both tension and compression individually) and are formulated as:

$$\mathbf{KU} = \mathbf{F} \tag{3}$$

$$\frac{c(\boldsymbol{\rho})}{c_L} \leq 1, \quad c(\boldsymbol{\rho}) = \sum_{e=1}^{N} \mathbf{U_e^T K_e U_e}, \; c_L = a_c c_0, \tag{4}$$

$$u^e_{max} < \frac{1}{500} l, \quad e \in \Omega_{des} = \Omega_{mat} \subseteq R^n, \; n = 2 \tag{5}$$

$$\rho_e^{(p-q)} \left(\frac{\sigma_{comp,e}}{\sigma_{comp,lm}} \right) \leq 1, \quad e = 1, 2, \ldots, N \tag{6}$$

$$\rho_e^{(p-q)} \left(\frac{\sigma_{ten,e}}{\sigma_{ten,lm}} \right) \leq 1, \quad e = 1, 2, \ldots, N \tag{7}$$

where $\boldsymbol{\rho}$ is the vector of the pseudo-densities[2]; $\mathbf{K}$, $\mathbf{K_e}$ are the global and element stiffness matrices, which are functions of $E(\rho_e)$; $\mathbf{U}$, $\mathbf{U_e}$ are the global and element matrices referring to the nodal displacements; $\mathbf{F}$ is the global load matrix; c_0 is the compliance calculated for the full domain; c_L is the allowable compliance limit; α_c is the respective fraction percentage; μ is the Poisson's ratio; u^e_{max} is the maximum nodal displacement; l is the total length of the structure under consideration here; q is the exponent related to the 'qp' approach for stress constraint relaxation as discussed in [18, 19] in order to address the singularity problem [27] and avoid the creation of zero stresses in void elements; $\sigma_{comp,e}$ and $\sigma_{ten,e}$ are the compressive and tensile stresses extracted locally per finite element, respectively; and $\sigma_{comp,lm}$ and $\sigma_{ten,lm}$ are the compressive and tensile strength limits defined according to the glass material properties, respectively.

[2] All the variables highlighted in bold refer to vectors and matrices.

It is noted that only the constraints related to the displacement and principal stresses serve to ensure the structural integrity of the design and are directly formulated according to the glass material properties. The compliance constraint is mainly defined by the end user following a strategy as described in [19] and contributes to the overall performance of the algorithm by guiding the simulation faster to an optimal result.

The last constraint refers to the annealing time limit and is formulated according to the maximum length scale approach [26]. The maximum cross-sectional dimension d_{max} is defined through considering primarily the maximum dimension that can be annealed in the set time limit based on the respective annealing rate [4] and the glass composition input. In this light, input based on different glass types is applied to evaluate the extent to which such changes affect the final outcome. Lastly, the need for homogeneous mass distribution in the geometry is also considered as a maximum limit to prevent large cross-sectional differences and uneven cooling that could cause local stress concentrations and breakage right from the cooling process. In total, d_{max} is expressed as:

$$d_{max} = \min(d_{ann}, d_{hom}), d_{ann} = \sqrt{\frac{T_{ann,max}\sigma_{res}}{\Delta T \frac{E\alpha_{ex}}{1-\mu}\frac{\rho_{mat}c_p}{\lambda}b}} \tag{8}$$

where d_{ann} is calculated adopting the formula by CelSian Glass & Solar and refers to the maximum cross section to be annealed in the set time limit $T_{ann,max}$; d_{hom} is the maximum cross section to ensure homogeneous mass distribution; σ_{res} is the maximum allowable permanent residual stress in the glass article; ΔT is the annealing temperature range; α_{ex} is the thermal expansion coefficient; ρ_{mat} is the material density; c_p is the specific heat capacity; λ is the thermal conductivity; and b is a factor based on the shape of the cross section and its capability to radiate heat.

3 Numerical Results

3.1 Design Problem

The case study refers to a bridge spanning 4.20 m, whose demand of tensile strength poses an additional challenge to the optimization problem. Moreover, any compromised transparency due to the complexity of the optimized form can serve as an advantage in this case, as it prevents an influence in the depth perception of the visitors, which in turn could decrease their confidence while walking on a completely transparent glass surface. The overall shape, dimensions and boundary conditions are defined based on the needs of an interior bridge placed in the Great Court at the British museum [28]. Additionally, redundancy and safety issues are considered while defining the design strategy. The total slab is divided along the transversal axis into two identical monolithic components, while laminated float glass sheets cover their upper surface [29] (Fig. 2). The latter also prevent from direct impact stresses on the load-bearing glass structure, which can be equally critical with far-field stresses for glass articles due to the risk of activating initial defects and fracture mechanisms [30]. The design domain refers to the characteristic planar longitudinal profile of the individual monolithic component without the top glass sheets.

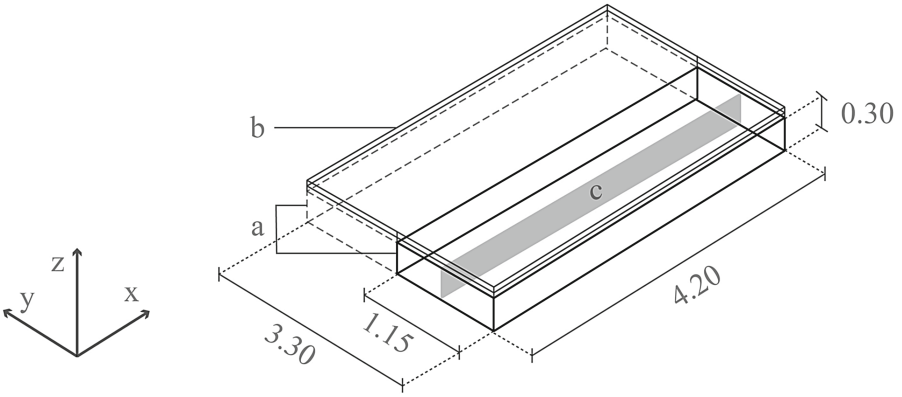

Fig. 2. Design strategies for redundancy and safety: (a) Division into two individual components (b) Float glass sheets (c) Design domain Ω_{des}.

Table 1. Permanent (p) loads, live (l) loads, and safety factors.

Self-weight of slab (p) (kN/m^2)	Float glass sheets (p) (kN/m^2)	People (l) (kN/m^2)	Maintenance (l) (kN/m^2)	Safety factor – permanent loads	Safety factor – live loads
9.8	1.2	5	0.4	1.2	1.5

The respective permanent and live loads are applied uniformly at the upper surface of the design domain according to Eurocode 1, Chapter 6 for museums (Table 1). They are only applied along the vertical direction since any lateral loads, such as due to wind, are eliminated, given that the example refers to an interior slab.

3.2 Optimization Formulation

For the finite element modeling, symmetry in terms of design domain, load application and boundary conditions is exploited, in order to reduce the total computational time and power needed for the algorithm to converge and, thus, improve its performance. The mesh is divided into 3150 quadrilateral finite elements (0.02 m * 0.02 m), but only half of the respective pseudo-density values are inserted as design variables in the optimization solver. The total structure is generated as a reflection of them along the middle transversal axis of the design domain (Fig. 3). Additionally, the constraints are evaluated only on specific critical nodes and elements each time. Particularly, the displacement is evaluated only on the upper middle node, whereas the manufacturing and stress constraints are evaluated locally in each finite element of the half-domain to ensure continuity and efficiently avoid local peak values. Compliance is evaluated as a global constraint for the total structure.

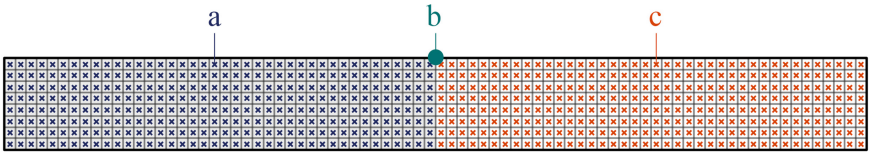

Fig. 3. Design domain Ω_{des} with (a) finite elements related to design variables and evaluation of manufacturing and principal stresses constraints, (b) critical node for displacement constraint, (c) symmetric domain.

3.3 Results

The following examples illustrate the practicality and versatility of the implementation by showcasing how input related to distinct parameters, such as glass composition and design strategies, affects the final outcome (Table 2). Regarding the glass composition, the most prevailing two types are applied: borosilicate and soda-lime glass. They share similar mechanical and structural properties, but they have considerably different thermal properties [6] requiring different annealing durations for the same geometry. Particularly, borosilicate glass has significantly lower thermal expansion coefficient, thus, cooling down approximately three times faster than soda-lime glass (Table 3).

All the examples share the same constraints, though adjusted to reflect the input conditions each time (Table 4). In this light, given that casting is applied, the value of the design tensile strength is compromised comparing to laminated glass because of casting defects and fracture mechanism risks [6]. Regarding the compliance constraint, different fractions are used based on the compliance of the full initial design domain. The rest of the input values related to the optimization are summarized in Table 5.

Table 2. Overview table with input conditions for each example.

Name[a]	Glass composition	Supports	Cross section height (cm)
BR-PN-30	Borosilicate	Point	30
SL-PN-30	Soda-lime	Point	30
BR-FX-30	Borosilicate	Fixed	30
BR-PN-40	Borosilicate	Point	40

[a]The acronyms refer to the glass composition (BR: Borosilicate/SL: Soda-lime); the edge support conditions (PN: Point/FX: Fixed); and the cross section height in cm

Table 3. Input values per glass composition.

	Density (kg/m^3)	Poisson's ratio (−)	Annealing temperature range (K)	Thermal expansion coefficient (1/K)	Thermal conductivity (W/(m*K))	Specific heat capacity (J/(kg*K))
Borosilicate	2500	0.2	70	$3.25*10^{-6}$	1.15	800
Soda-lime	2500	0.2	68	$8.5*10^{-6}$	1.06	870

Table 4. Values used for constraints evaluation.

Design tensile strength[a] (MPa)	Design compressive strength (MPa)	Displacement (m)	Compliance[b] (kNm)	Max annealing time (s)
6.4	500	0.0084 (length/500)	4 $c_0 = 0.0184$ (h = 0.30 m) 6.5 $c_0 = 0.0182$ (h = 0.40 m)	432000 (5 days)

[a]Calculated based on the German structural design standard in glass constructions (DIN18008), and additional compromises capturing potential casting defects applied according to [6, 30]
bThe percentages related to the compliance fraction are defined through trial and error for each cross section size. They serve to guide the algorithm faster to feasible solutions [19], but are relaxed to avoid convergence to local minima

Table 5. Input values for optimization setup.

Young's modulus E (GPa)	Young's modulus lower bound E_0 (GPa)	Penalization value p (−)	Stress relaxation value q (−)[a]	Maximum residual stress σ_{res} (MPa)	Shape factor b (−)
70	0.00001	3	2.8	1	0.3

[a]The value used for the q exponent is defined following the approach in [19]

As seen in Fig. 4, the algorithm converges to clear shapes without large grey zones which would be difficult to interpret physically. Therefore, it yields realistic optimal results that have active all the constraints posed in the formulation.

Among the different results, it is evident that the most influential input parameter is the support condition. Hence BR-FX-30 is the only shape variation which differs substantially from the first run BR-PN-30, whereas the rest can be observed as variations of the initial result. Therefore, the main design principles in all optimization runs with point supports stay the same. The resulting shapes consist of a main arc-shape part and a secondary lattice structure at the bottom that increases the total structural stiffness. Additionally, subtle nerves are developed on the top part of the arc to transfer the uniform loads effectively from the top surface to the load bearing structure.

Name	Optimization Result [a]	Volume (m^3)	Annealing time (hours : minutes) [b]
BR-PN-30		0,690	35:00
SL-PN-30		0,738	55:20
BR-FX-30		0,419	18:30
BR-PN-40		0,443	23:30
Compact slab (h = 17 cm)		0,821	83:30 (BR) 249:50 (SL)

[a] The resulting shapes are illustrated in a black-white gradient that reflects the existence (black) or absence (white) of material according to the pseudo-density value of each finite element.
[b] The estimated time refers only to the annealing phase proposed by [4] and not to the total cooling time needed.

Fig. 4. Optimization results for different design input variations.

However, there are small adjustments to effectively address the specific input situation in each case. Firstly, in SL-PN-30 the algorithm does not converge to a result with the main arc part as thick as in BR-PN-30, but it details it into a larger number of thinner elements. Therefore, the characteristic cross-sectional dimension of the geometry becomes smaller allowing for annealing time that lies inside the imposed limit, despite the higher thermal expansion coefficient of soda-lime glass.

Additionally, in the case of a larger profile height (BR-PN-40), a clearer formation of the main arc and the respective Y-shaped nerves is achieved. The outcome of this optimization run has the clearest boundary of all counterparts. The only variation that converges to a considerably different result than the initial arc shape is BR-FX-30. In this case, the structure is analyzed into three different parts: two cantilevers[3] on the sides which support a lattice structure placed in the middle part. As earlier, small nerves are created between the different parts to transfer surface loads. Besides the slenderness of the individual elements, the performance of the component lies well inside the limitations related to buckling, which is an important issue for glass articles and can lead to failure.

All the optimization outcomes are considerably more lightweight compared to the reference slab, i.e. the thinnest full material slab that could be applied and still comply with the principal stresses and displacement restrictions (height = 0.17 m). Particularly, the volume reduction achieved through optimization ranges between 10–49% of the reference volume whereas the annealing time needed can be reduced by up to 78%.

[3] The geometry of the cantilevers resembles the shape of the classical MBB-Beam problem when similar boundary conditions are imposed [33].

The heaviest outcome comes from the SL-PN-30 variation where, because of the soda lime glass composition, the resulting geometry consists of a larger number of elements compared to BR-PN-30. This is caused by the high thermal expansion coefficient of soda lime glass that renders the thick cross sections not feasible to be annealed in the posed time limit and, thus, they must be analyzed in more elements, which eventually result in increased total structural volume. In contrast, the lighter outcome is related to the BR-FX- 30 variation accounting for almost one half of the volume of the reference slab. Besides the large number of elements in this case, the overall thinner dimensions decrease the overall mass and ensure better performance in terms of annealing time.

In total, this exploration showcases the practicality of the implementation, since the algorithm maintains the design principles that correspond to the optimum result but adjusts the material distribution to respond to the different input conditions. Therefore, it can assist profoundly the design process altering the optimization outcome to meet the specific needs of each space while complying with the set of the posed criteria.

4 Application

4.1 Design Strategy

The optimization outcome from BR-FX-30 variation (Fig. 5) achieves the largest volume and annealing time reduction while at the same time performs efficiently regarding structural performance. Therefore, it is selected to be applied to the slab design.

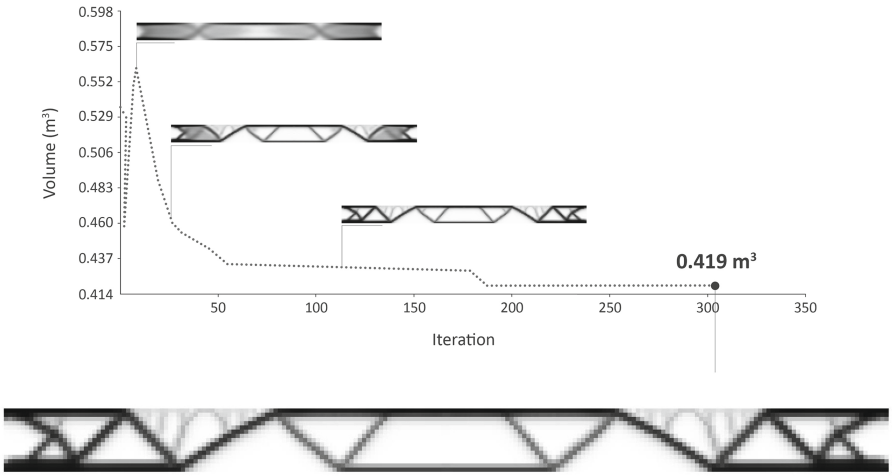

Fig. 5. Convergence diagram for the BR-FX-30 variation outcome selected.

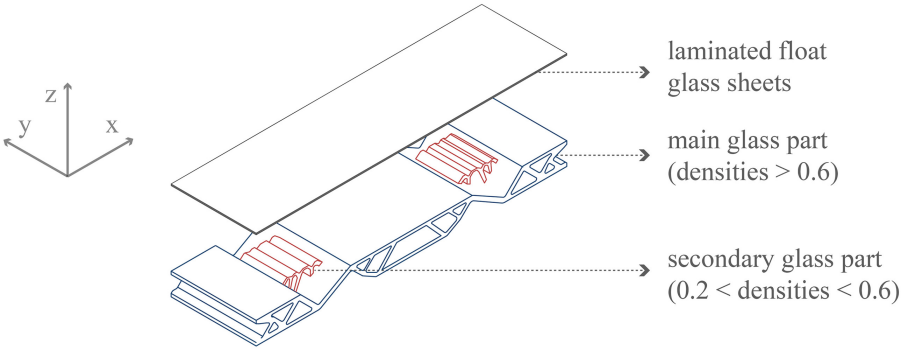

Fig. 6. Design strategy diagram.

To validate the structural performance of the geometry, the planar optimized cross section is translated into a 3-dimensional shape, through its extrusion along the *y* axis. The contribution of each finite element to the total volume is proportional to its contribution to the structural stiffness during the optimization which is reflected to the respective assigned values of the pseudo-densities. Therefore, the elements that correspond to densities above 0.6 are extruded through the whole width, whereas elements with densities between 0.2–0.6 are only extruded through half of it. Lastly, the laminated float glass sheets are applied on the upper surfaces of the components (Fig. 6).

4.2 Structural Evaluation

The performance of the total structure, both the monolithic component and the float glass sheets on top, is evaluated with the use of Ansys software[4]. The factors which are evaluated are the displacement and principal stresses, regarding both tension and compression. The results (Table 6) validate the optimization process since the values of all factors are well inside the allowable limits (Table 4).

Table 6. Results of structural verification with Ansys.

Displacement (m)	Tensile stress (MPa)	Compressive stress (MPa)
0,00012	2,96	5,56

[4] Only one of the two monolithic glass components is evaluated structurally in Ansys since the two parts are assumed to perform individually.

4.3 Fabrication

Although permanent steel molds are generally preferred for casting series of high-precision glass elements, the geometrical complexity and customization of the TO geometries renders their use unsuitable in this case[5], pointing towards the direction of using disposable molds as the most promising solution. Particularly, in glass art, large-scale customized castings employ the lost wax technique to produce disposable silica plaster molds which are later used for kiln-casting the components [1]. Yet, this method, is unfavored in our case due to the lengthy, complex, and laborious mold fabrication process [31] as well as compromised dimensional accuracy.

In this light, 3d printed sand molds, which are typically used for metal castings and are recently employed in castings of optimized concrete members [32], are suggested as a solution with large potential for complex glass applications to achieve lower overall cost, higher shape precision and fast fabrication process [2, 3, 8]. Additionally, they are water dissolvable facilitating the unmolding process, while the remaining sand can also be reused. Relevant research by TU Delft [8] already showcases the potential of using 3d printed sand molds made with inorganic binders for kiln glass casting. However, it also highlights the need for further research to refine technical aspects, such as the identification of a coating that allows for a completely transparent surface quality [8], which reduces the need for post-processing and improves the shape precision. Some first promising results in this direction have been recently published by ETH [31], bringing us a step closer to the realization of such complex cast glass structures (Fig. 7).

Fig. 7. Visualization of the final outcome.

[5] Although multi-component steel molds can be made for the manufacturing of complex parts, they cannot produce undercuts because the mold must be eventually removed.

5 Conclusions

This paper introduces a new integrated TO formulation combining structural and manufacturing constraints within a unified nonlinear programming statement seeking to enable the design of feasible monolithic large cast glass structures. This can change completely the perception of glass as building material offering unique spatial qualities and enriching profoundly the vocabulary of architectural forms, by introducing aesthetic and structurally sound 3-dimensional glass structures.

The developed formulation is versatile and robust to input alterations. This is showcased through the application of different input conditions regarding the glass composition and the design strategies, which proved that the proposed setting results into robust solutions that comply with all the imposed constraints. Considerably different shapes and volume reduction is achieved based on the glass type and the design strategies applied. Volume reduction ranges between 10–49% compared to the optimal full-material cross section, i.e. the thinnest slab ensuring sufficient structural performance. Similarly, annealing time is reduced up to 78% compared to the reference optimal slab, ultimately rendering the structures more feasible to manufacture.

Overall, this study highlights the potential of using TO as a practical tool in the early design phase leading to better performing and non-intuitive architectural solutions. This diminishes the need for post-processing, shortening the design cycle and allowing for better interconnection between the different specialists involved in the building industry. Future research may focus on incorporating to the formulation practical fabrication-related limitations, such as minimum void dimension to ensure sufficient mold stiffness and integrating additional aspects, such as evaluation of the displacement of the upper laminated float glass sheets or evaluation of second-order structural effects. Moreover, additional design criteria can be considered, such as the establishment of areas in the geometry where the complexity of the form is restricted to allow for increased transparency through minimizing the visual distortions. Finally, to evaluate and improve the accuracy of the developed algorithm, it is important that the numerical results are coupled with mechanical tests on corresponding prototypes. The proposed implementation can be further expanded to other brittle materials, such as unreinforced concrete, and other fabrication methods, such as 3d printing.

Acknowledgements. The authors would like to thank ir. Hans Hoogenboom (Digital Technologies section) at the VR-lab at TU Delft Faculty of Architecture & the Built Environment and Aytac Balci (@Hok Student ICT Support) for offering the facilities and support for the computational needs of this research. Dr. Andriotis would further like to acknowledge the support by the TU Delft AI Labs program.

References

1. Oikonomopoulou, F., Bristogianni, T., Barou, L., Veer, F., Nijsse, R.: The potential of cast glass in structural applications. Lessons learned from large-scale castings and state-of-the art load-bearing cast glass in architecture. J. Build. Eng. **20**, 213–234 (2018)

2. Oikonomopoulou, F., Koniari, A., Damen, W., Koopman, D., Stefanaki, I., Bristogianni, T.: Topologically optimized structural glass megaliths: potential, challenges and guidelines for stretching the mass limits of structural cast glass. In: 8th Eighth International Conference on Structural Engineering, Mechanics and Computation (2022)
3. Damen, W., Oikonomopoulou, F., Bristogianni, T., Turrin, M.: Topologically optimized cast glass: a new design approach for loadbearing monolithic glass components of reduced annealing time. Glass Struct. Eng. (2022)
4. Shand, E., Armistead, W.: Glass Engineering Handbook, New York (1958)
5. Schober, H., Schneider, J., Justiz, S., Gugeler, J., Paech, C., Balz, M.: Innovations with Glass, Steel and Cables. Tampere, Finland (2007)
6. Oikonomopoulou, F.: Unveiling the third dimension of glass. Solid cast glass components and assemblies for structural applications (2019)
7. Zirker, J.: An Acre of Glass: A History and Forecast of the Telescope. JHU Press (2005)
8. Oikonomopoulou, F., Bhatia, I., van der Weijst, F., Damen, W., Bristogianni, T.: Rethinking the cast glass Mould. An exploration on novel techniques for generating complex and customized geometries. In: Challenging Glass 7 Conference on Architectural and Structural Applications of Glass (2020)
9. Langelaar, M.: Topology optimization of 3D self-supporting structures for additive manufacturing. Addit. Manuf. **12**, 60–70 (2016)
10. Luo, Y., Sigmund, O., Li, Q., Liu, S.: Additive manufacturing oriented topology optimization of structures with self-supported enclosed voids. Comput. Methods Appl. Mech. Eng. **372** (2020)
11. Duysinx, P., Sigmund, O.: New developments in handling stress constraints in optimal material distributions. In: 7th AIAA/USAF/NASA/ISSMO Symposium on Multidisciplinary Analysis and Optimization (1998)
12. Le, C., Norato, J., Bruns, T., Ha, C., Tortorelli, D.: Stress-based topology optimization for continua. Struct. Multidiscip. Optim. **41**, 605–620 (2010)
13. Paris, J., Navarrina, F., Colominas, I., Casteleiro, M.: Topology optimization of continuum structures with local and global stress constraints. Struct. Multidiscip. Optim. **39**, 419–437 (2009)
14. Yang, R., Chen, C.: Stress-based topology optimization techniques. Struct. Optimiz. **12**, 98–105 (1996)
15. Duysinx, P., Bendsoe, M.: Topology optimization of continuum structures with local stress constraints. Int. J. Numer. Meth. Eng. **43**, 1453–1458 (1998)
16. Giraldo-Londoño, O., Paulino, G.: A unified approach for topology optimization with local stress constraints considering various failure criteria: von Mises, Drucker–Prager, Tresca, Mohr–Coulomb, Bresler–Pister and Willam–Warnke. Proc. Roy. Soc. A **476** (2020)
17. Senhora, F.V., Giraldo-Londoño, O., Menezes, I.F.M., Paulino, G.H.: Topology optimization with local stress constraints: a stress aggregation-free approach. Struct. Multidiscip. Optim. **62**(4), 1639–1668 (2020). https://doi.org/10.1007/s00158-020-02573-9
18. Bruggi, M.: On an alternative approach to stress constraints relaxation in topology optimization. Struct. Multidiscip. Optim. **36**, 125–141 (2008)
19. Bruggi, M., Duysinx, P.: Topology optimization for minimum weight with compliance and stress constraints. Struct. Multidiscip. Optim. **46**, 369–384 (2012)
20. Luo, Y., Kang, Z.: Topology optimization of continuum structures with Drucker-Prager yield stress constraints. Comput. Struct. **90–91**, 65–75 (2012)
21. Bruggi, M., Duysinx, P.: A stress–based approach to the optimal design of structures with unilateral behavior of material or supports. Struct. Multidiscip. Optim. **48**, 311–326 (2013)
22. Bendsoe, M.: Optimal shape design as a material distribution problem. Struct. Optim. **1**, 193–202 (1989)

23. Sigmund, O., Petersson, J.: Numerical instabilities in topology optimization: a survey on procedures dealing with checkerboards, mesh-dependencies and local minima. Struct. Optim. **16**, 68–75 (1998)
24. Bendsøe, M.P., Sigmund, O.: Topology Optimisation. Theory, Methods and Applications. Springer, Heidelberg (2004). https://doi.org/10.1007/978-3-662-05086-6
25. Sigmund, O.: A 99 line topology optimization code written in Matlab. Struct. Multidiscip. Optim. **21**(2), 120–127 (2001). https://doi.org/10.1007/s001580050176
26. Guest, J.: Imposing maximum length scale in topology optimization. Struct. Multidiscip. Optim. **37**, 463–473 (2009)
27. Cheng, G., Guo, X.: E-relaxed approach in structural topology optimization. Struct. Optim. **13**, 258–266 (1997)
28. Koniari, A.M.: Just Glass. Development of a Topology Optimization Algorithm for a Mass-Optimized Cast Glass Component. Delft University of Technology (2022)
29. Stefanaki, I.M.: Glass Giants. Mass-Optimized Massive Cast Glass Slab. Delft University of Technology (2020)
30. Bristogianni, T., Oikonomopoulou, F., Yu, R., Veer, F., Nijsse, R.: Exploratory study on the fracture resistance of cast glass. Int. J. Struct. Glass Adv. Mater. Res. **5** (2021)
31. Giesecke, R., Dillenburger, B.: Three-dimensionally (3D) printed sand molds for custom glass parts. Glass Struct. Eng. **7**, 231–251 (2022)
32. Jipa, A., Bernhard, M., Meibodi, M., Dillenburger, B.: 3D-printed stay-in-place formwork for topologically optimized concrete slabs. In: TxA Emerging Design + Technology Conference, San Antonio, Texas, USA (2016)
33. Liu, K., Tovar, A.: An efficient 3D topology optimization code written in Matlab. Struct. Multidiscip. Optim. **50**, 1175–1196 (2014)